Quantum Mechanical Bound States of the Yukawa Potential

A Thesis
Presented to
The Division of Mathematics and Natural Sciences
Reed College

In Partial Fulfillment
of the Requirements for the Degree
Bachelor of Arts

Ellen M. McManis

May 2012

Approved for the Division
(Physics)

_____

Nelia Mann

Acknowledgements

In the completion of this thesis, a profound debt is owed:

To my adviser, Nelia Mann, for all the help, support, and knowledge. To Mary James, for the help learning how to learn.

To my friends. To my classmates and fellow Reedies, who shaped me into the person who wrote this. To the upperclassmen (Reuven, Rosie, Robin, and Mary) who took the time, my freshman year, to tell me how neat physics was. To Joel Franklin, for sharing neat problems and his excitement for the subject.

To everyone on IRC who's been listening to my thesis ramblings these past months. And finally, to those people who have loved and supported me through this year.

You people are amazing.

Table of Contents

List of Tables

List of Figures

Abstract

We obtain a model for the relationship between the number of bound states of the Yukawa potential and $\lambda = \ell/\alpha$, the ratio of the exponential cutoff length scale to the "Bohr radius" for the problem. We use a semi-classical approximation to make a qualitative prediction for the relationship. We then use the finite difference method to obtain numerical values for the critical values λ_n, which are the values of λ at which the nth new bound state appears. These can be fit to a quadratic function, giving us $\lambda_n = A(l) + B(l)n + C(l)n^2$, where A, B, and C are constants that depend on the angular momentum quantum number l.

Introduction

The Yukawa potential describes a force mediated by a massive particle. It is

$$V(r) = -\frac{C}{r}e^{-r/\ell}, \tag{1}$$

where C and ℓ are constants. C sets the strength of the force; ℓ acts as a length scale. The exponential term provides an effective cutoff for the associated force: once r gets much larger than ℓ, the exponential term drops off quite rapidly. We are interested in how the bound states of a particle subject to this potential change with these constants.

The length scale of the potential, which limits the range at which the force acts, is related to the mass of the mediating particle m by the equation

$$\ell = \frac{\hbar}{mc}. \tag{2}$$

Both the mass m and the strength of the force C depend on the application of the potential. Most commonly, we use this potential to describe the force between protons and neutrons in an atomic nucleus, where m is the mass of the pion.

In general, to find the bound states of a particle under the influence of some $V(r)$, we solve the time-independent Schrödinger wave equation,

$$-\frac{\hbar^2}{2\mu}\nabla^2\psi(r,\phi,\theta) + V(r)\psi(r,\phi,\theta) = E\psi(r,\phi,\theta), \tag{3}$$

and look for solutions which go to zero at infinity. With the Yukawa potential, this equation cannot be solved analytically. However, in the limit where $r \ll \ell$, the exponential term disappears, leaving

$$V(r) \approx -\frac{C}{r}. \tag{4}$$

This is the same form as the Coulomb potential, which we use to find the bound states of an electron and a proton in hydrogen (for $C = \frac{e^2}{4\pi\epsilon_0}$). (4) suggests that we will be able to gain some insight into the Yukawa potential by looking at the solutions to the wave equation for the Coulomb potential.

These solutions can be written as [1]

$$\psi_{l,m_l,n}(r,\theta,\phi) = R_{n,l}(r)Y_{l,m_l}(\theta,\phi). \tag{5}$$

Here, l, m_l, and n are quantum numbers. The Y_{l,m_l} are the spherical harmonics. For simplicity, we begin by focusing on states with zero angular momentum, for which the solutions are spherically symmetric. For convenience, we introduce a length scale,

$$\alpha = \frac{\hbar^2}{C\mu}, \tag{6}$$

which is a constant with units of length. In hydrogen this is the Bohr radius, and reduces to the familiar $a_o = \frac{4\pi\epsilon_0\hbar^2}{\mu e^2} = 5.3 \times 10^{-11}$ m.

The simplest nucleus we might use the Yukawa potential for is that of deuterium. In deuterium, $C = 1.10286 \times 10^{-26}$ J m[1] and $\mu = m_p/2$, giving an α of 1.20×10^{-15} m. This is interestingly on the same order as $\ell = 1.46 \times 10^{-15}$ m, the cutoff length scale, which we obtain from (2) using $m = m_\pi = 135$ MeV/c^2.

We can now take $Y_{0,0} = 1/\sqrt{4\pi}$, leaving us with

$$\psi_{n,l=0}(r) = \frac{1}{\sqrt{4\pi}} R_{n,l=0}(r) = \frac{1}{\sqrt{4\pi}} e^{-r/\alpha n} L_{n-1}\left(2\frac{r}{\alpha n}\right) \tag{7}$$

where L_{n-1} is a Laguerre polynomial. The factor of $e^{-r/\alpha n}$ ensures that the wave function goes to 0 as r goes to infinity, with n controlling how fast that happens. The Laguerre polynomial determines how many nodes the wave function has. Because L_{n-1} has $n-1$ roots, the wave function will have $n-1$ nodes (figure 1).

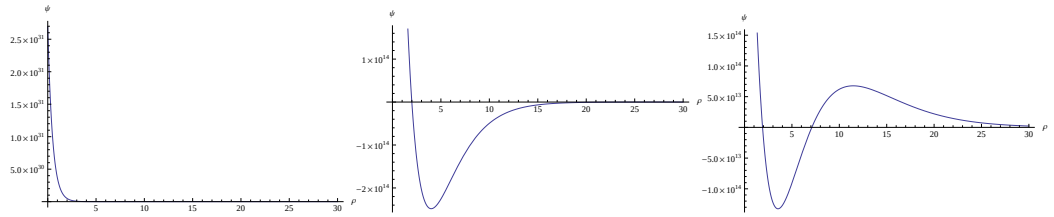

(a) $n = 1$ (b) $n = 2$ (c) $n = 3$

Figure 1: The first three bound states of $\psi(\rho)$ for the Coulomb potential, where $\rho = r/\alpha$. These show the nodes given by the Laguerre polynomials as well as the exponential dieoff of the wave function.

The energy for the particle described by this wave function is just a function of n (the principal quantum number), and is equal to

$$E_n = -\frac{C}{2\alpha n^2}. \tag{8}$$

There are an infinite number of bound states labelled by n, and as n gets large, the energies given by (8) get closer and closer to zero but never quite reach it (the states remain bound). As this happens, the wave functions can be found further and further from the origin. This effect can be seen in figure 2, in which the first four bound states are plotted.

[1]This value was obtained by using the numerical methods described in Chapter 2 to work backward from the known value of the length scale and the mass defect of deuterium, which will be equal to the energy of the ground state of the system.

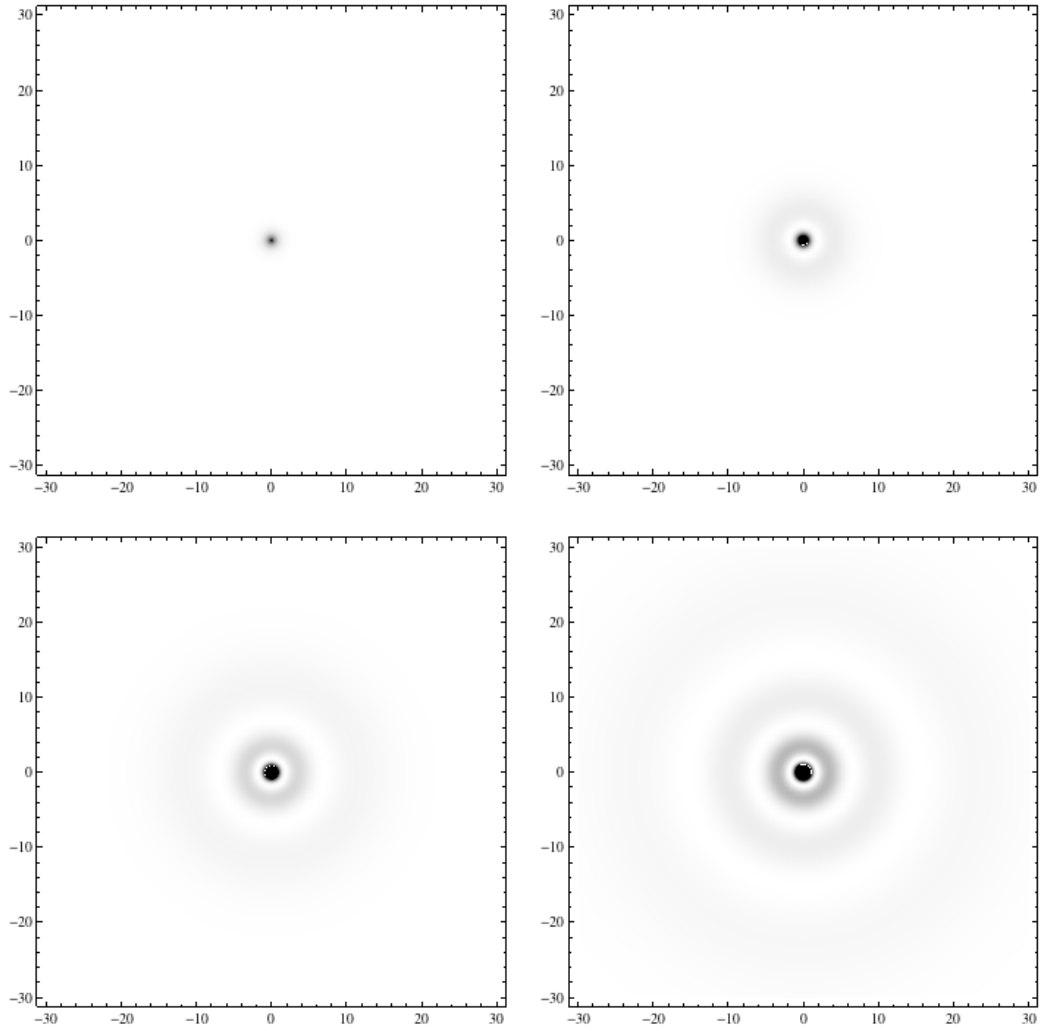

Figure 2: The first four spherically symmetric wave functions. This plot shows the probability density, $\psi(\rho)^2$, in the x-y plane. Again, $\rho = r/\alpha$ is the non-dimensionalized radial coordinate.

Now let us consider how this changes for the Yukawa potential, which itself has an exponential die-off with length scale ℓ. Because of (4), we expect the Yukawa states to resemble the Coulomb states for bound states with $r \ll \ell$. For $r \gg \ell$, the potential is approximately 0. We do not expect to find any bound states where the wave function is significantly non-zero in this region, because there is no force to bind the particle. We therefore expect that the number of bound states of this potential will be be finite.

When working with the Yukawa problem, we will continue using the length scale α from (6). What we are interested in is not ℓ itself, but the ratio ℓ/α which we call λ. If λ is small, a given state is more likely to fall outside of the range of the potential, meaning that only a small number of states (those whose wave functions do not extend very far out) may be bound. For a large λ, the reverse is true, and we expect a large number of bound states.

To find the relationship between the number of bound states and λ, we will use the finite difference method to solve the Schrödinger equation in chapter 2. Because we are explicitly working around the area where $r \approx \ell$, an analytic approximation by perturbing the Coulomb potential [2] will not give us much insight into what we expect our numerical results to be. Instead, in chapter 1 we use the Bohr method to obtain an idea of what we expect.

Chapter 1

Semi-Classical Approximation

To better understand the relationship between the number of bound states and ℓ, we begin with a semi-clasical approximation. This will give us an idea what to expect from the numerical analysis in chapter 2.

1.1 The Bohr Model

For this approximation we can again exploit the similarities between the Yukawa potential and the Coulomb potential and use the Bohr model. The postulates of the model include the following:

1. Particles move in circular orbits around the center under the influence of some potential $V(r)$. They obey all the laws of classical mechanics.

2. Angular momentum is quantized; $L = n\hbar$ where n is a positive integer.

To use these postulates, first we look at the classical energy of a particle moving under the influence of a potential:

$$E = \frac{1}{2}\mu\dot{r}^2 + \frac{L^2}{2\mu r^2} + V(r) = \frac{1}{2}\mu\dot{r}^2 + \frac{1}{2}\frac{(n\hbar)^2}{\mu r^2} + V(r). \tag{1.1}$$

We can roll the second half of the equation up into an effective potential, producing something of the form $E = KE + PE$. The effective potential V_{eff} is then

$$V_{\text{eff}}(r) = \frac{(n\hbar)^2}{2\mu}\frac{1}{r^2} + V(r). \tag{1.2}$$

Referring back to the first postulate, we know that our semi-classical particle is moving in a circular orbit. Classically, a circular orbit occurs when the effective potential is minimized, that is, when

$$\frac{dV_{\text{eff}}}{dr}\Big|_{r=r_0} = 0. \tag{1.3}$$

Given some n, the radius of the Bohr orbit will be given by (1.3). The energy of this orbit can be obtained by evaluating (1.1) at r_0. Because the orbit is circular, $\dot{r} = 0$,

so the energy will be

$$E_n = \frac{1}{2}\frac{(n\hbar)^2}{\mu r_0^2} - V(r_0). \tag{1.4}$$

1.2 Application to Coulomb Potential

Let's remind ourselves how this works for the Coulomb potential. To make this easier to work with, we define a nondimensionalized radial coordinate

$$\rho \equiv \frac{r}{\alpha} \tag{1.5}$$

using the length scale from (6), the "Bohr radius" for this problem. We also define a time scale:

$$\beta \equiv \frac{C^2 m}{\hbar^3}. \tag{1.6}$$

We can substitute these into (1.1) and (1.2) in order to obtain

$$\frac{2\alpha}{C}E = \tilde{E} = \rho'^2 + \frac{n^2}{\rho^2} - \frac{2}{\rho}, \tag{1.7}$$

$$\tilde{V}_{\text{eff}} = \frac{n^2}{\rho^2} - \frac{2}{\rho}. \tag{1.8}$$

We can plot the effective potential as a function of ρ (figure 1.1). The circular orbits will be at the minimum of this effective potential, where the radius of the particle's orbit is constant. The value of the energy is then $\tilde{V}_{\text{eff,min}}$. Note that a different value of n gives a different effective potential with a different minimum.

To find the location of this minimum, we differentiate (1.8) and set the result to 0, which gives

$$\rho_0 = n^2. \tag{1.9}$$

Plugging this into (1.7), we find that the energy of the particle in this orbit is

$$\tilde{E} = -\frac{1}{n^2}. \tag{1.10}$$

For the Coulomb potential, this is perfect – the semi-classical Bohr model gives exactly the same energy spectrum as we would obtain by solving the Schrödinger equation, despite the inappropriate use of classical mechanics. In other quantum systems, a Bohr approach generally gives a qualitatively reasonable result that's off by a bit quantitatively. For example, when the three-dimensional simple harmonic oscillator is studied, the Bohr method obtains the right form of the spectrum, but it differs from the actual spectrum by an offset of the ground state energy. For the logarithmic potential, the Bohr spectrum (with appropriate nondimensionalization) is $\tilde{E}_n = \frac{1+\ln(2)}{2} + \ln(n)$, while the numerically determined quantum spectrum is in the form $\tilde{E}_n = A + \ln(n + B)$ for some constants A and B [3].

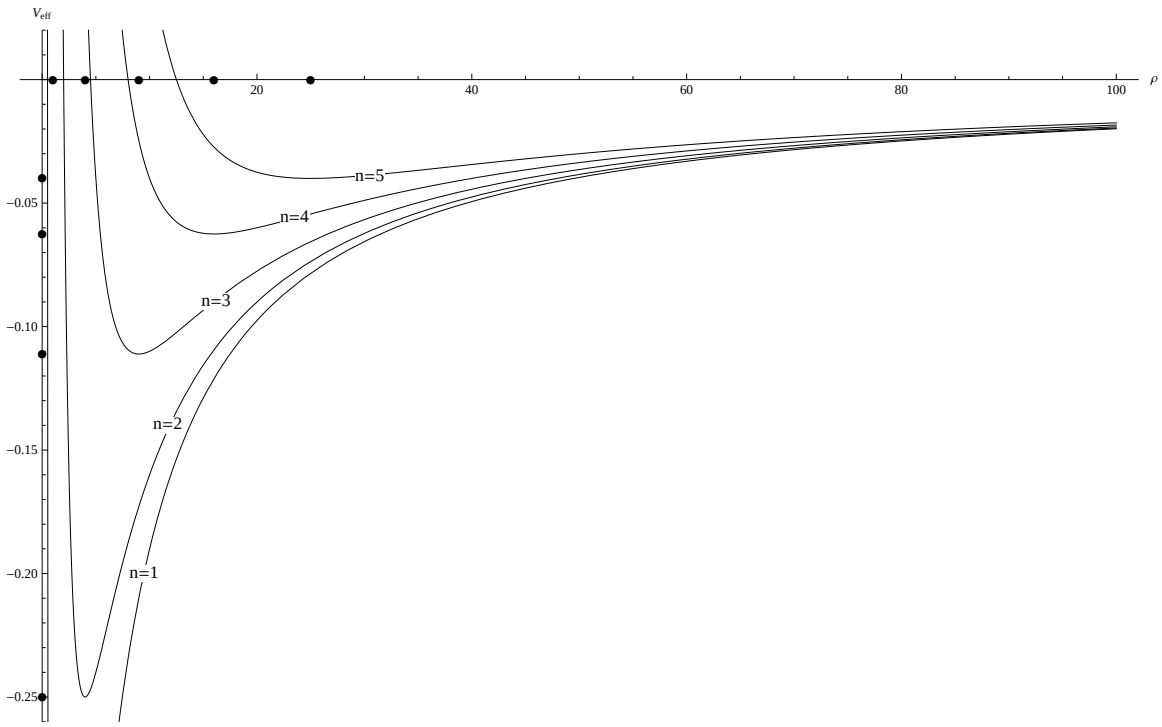

Figure 1.1: The effective Coulomb potential. Particles can exist with energies greater than the potential energy, and their trajectories will cover all possible radii at that energy. The black dots on the ρ axis indicate the minima of the curves, where circular orbits exist. The dots on the V_{eff} axis indicate the values of the energy at those minima.

1.3 Approximating the Yukawa Potential with a Cutoff

Returning to the the Yukawa potential, when $r \ll \ell$ we expect the $1/r$ behavior to dominate, and the potential to behave similarly to the Coulomb potential. When $r \gg \ell$, we expect the exponential term to dominate, and the potential to go to zero. As a naïve approximation of this behavior, we can consider cutting off the Coulomb potential at $r = \ell$. In keeping with the earlier nondimensionalization, we define $\lambda \equiv \frac{\ell}{\alpha}$. Our effective potential is now

$$\tilde{V}_{\text{eff}}(\rho) = \begin{cases} \frac{n^2}{2}\frac{1}{\rho^2} - \frac{1}{\rho} & : \rho \leq \lambda \\ 0 & : \rho > \lambda \end{cases} \tag{1.11}$$

This cutoff means that the relationship between ρ and n holds while $\rho < \lambda$, but breaks down after, limiting the number of bound states (figure 1.2). Any bound state allowed under (1.9) for which ρ exceeds λ will not exist. If we imagine increasing λ gradually, a new bound state will be added whenever we pass through a point $\lambda = n^2$ (for some integer n). We call these points the critical values of λ, notated λ_n, where n is a positive integer that corresponds to the number of bound states just above that critical value. Based on this treatment, we expect $\lambda_n = n^2$.

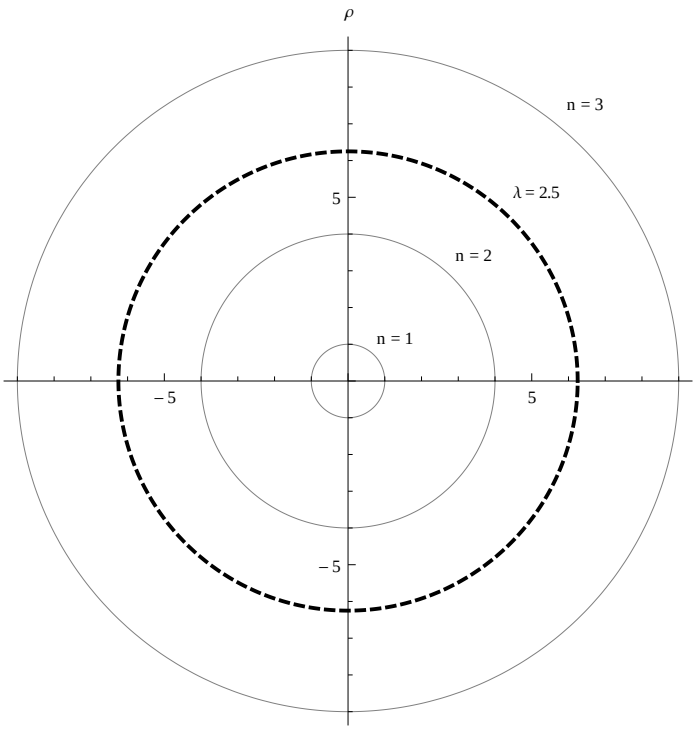

Figure 1.2: A polar plot of the first three Bohr orbits along with a cutoff at $\lambda = 2.5$. Because the $n = 3$ orbit lies outside the cutoff, it would not be allowed under (1.11).

1.4 Application to Yukawa Potential

To perform a more careful analysis of the potential, we look at the graph of its effective potential (figure 1.3):

$$\tilde{V}_{\text{eff}} = \frac{n^2}{\rho^2} - \frac{2}{\rho} e^{-\rho/\lambda}. \tag{1.12}$$

As before, we can see that bound states exist for some n and ρ where V_{eff} is less than 0, and these bound states include circular orbits at the minimum of V_{eff}. However, there also appear to be bound states *above* $E = 0$. Classically, these are perfectly valid orbits. Quantum mechanically, a particle in one of these states can tunnel through and become a scattering state. This gives us two possible definitions for a critical value of λ. The first is where the minimum of V_{eff} for some n moves below zero – that is, where the value of lambda allows an additional stable bound state ($E < 0$). The other occurs where V_{eff} for some n first starts to have a minimum at all, giving it a bound state with $E > 0$. These two critical points are shown in figure 1.4.

1.4.1 Stable bound states

The first of these critical values occurs when the minimum of V_{eff} is 0. We again start by taking the derivative of (1.12) and setting it to 0, obtaining

$$\left.\frac{dV}{d\rho}\right|_{\rho=\rho_0} = 0 = -\frac{2n^2}{\rho_0^3} + \frac{2}{\rho_0^2} e^{-\rho_0/\lambda} + \frac{2}{\rho_0 \lambda} e^{-\rho_0/\lambda}, \tag{1.13}$$

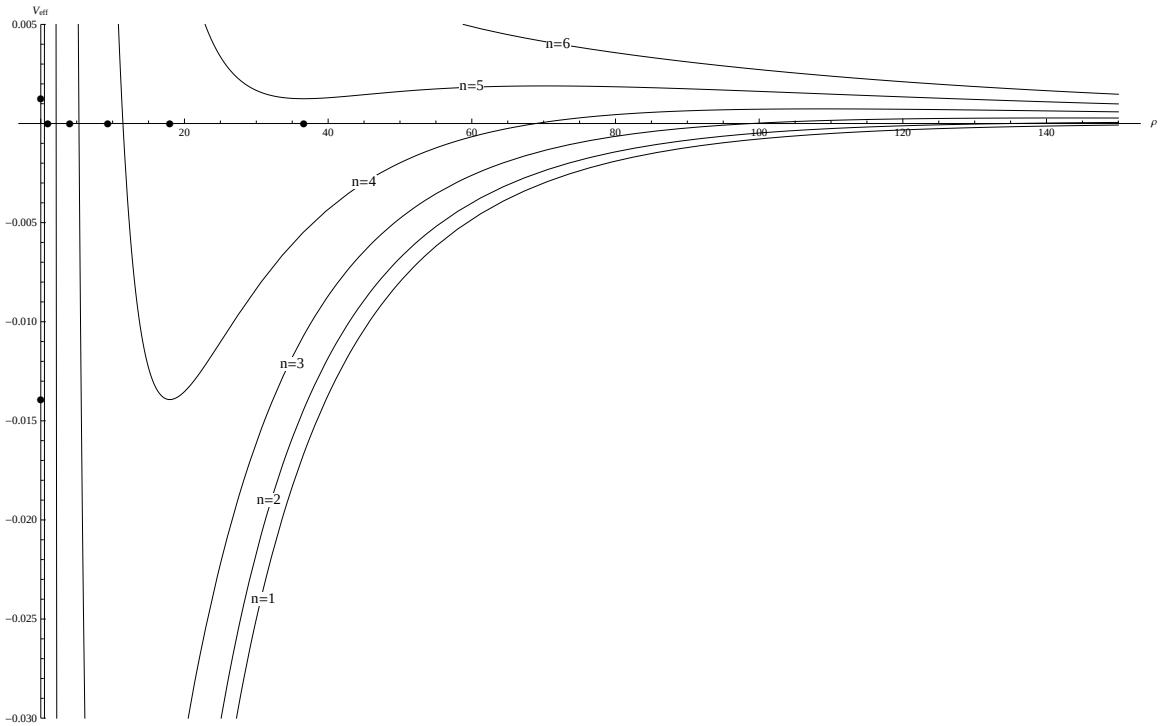

Figure 1.3: The effective Yukawa potential. (1.12) was plotted for $n = 1$ through 6 with $\lambda = 32$. As with Coulomb, the curves get increasingly shallow as n increases. The curves for $n = 1$ through 4 all have a circular orbit with $E < 0$, that is, they have a stable Bohr bound state. The curve for $n = 5$ has a very slight minimum, but it does not go below 0, corresponding to an unstable Bohr bound state. The $n = 6$ curve does not have a minimum at all. For all curves with a minimum, the approximate location of this minimum has been plotted on the ρ axis and the value of the energy at this minimum on the V_{eff} axis.

where ρ_0 is the value of ρ when V_{eff} is minimized. This equation holds for any λ and has no closed form solution, but we can find one for the specific case where λ is some critical value λ_n and $V_{\text{eff}}(\rho_0) = 0$. We solve the equation

$$V_{\text{eff}}(\rho_0) = 0 = n^2 - 2\rho_0 e^{-\rho_0/\lambda_n} \tag{1.14}$$

for n^2 and plug the result into (1.13), obtaining

$$\rho_0 = \lambda_n. \tag{1.15}$$

Plugging this back into the equation for $V_{\text{eff}}(\rho_0)$, we find that

$$\lambda_n = \frac{e}{2}\, n^2 \approx 1.36\, n^2, \tag{1.16}$$

which is pretty close to the $\lambda_n = n^2$ behavior we obtained earlier.

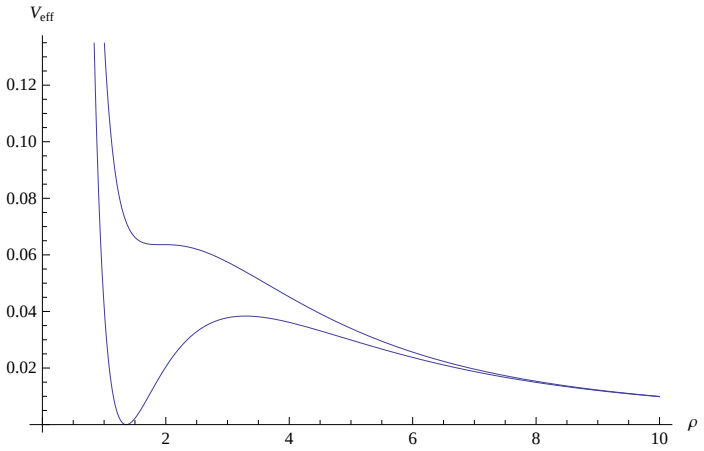

Figure 1.4: Two curves showing V_{eff} at the two critical values of λ – one where a new stable bound state appears, and one where a new bound state with $E > 0$ appears.

1.4.2 Unstable bound states

Having determined a formula for the λ_ns at which new bound states with $E < 0$ appear, we turn to the appearance of classically bound states with $E > 0$. A bound state exists when V_{eff} has a minimum. We found the ρ_0 where this minimum occurs in (1.13), which we can rewrite as

$$n^2 = \left(\rho_0 + \frac{\rho_0^2}{\lambda}\right) e^{-\rho_0/\lambda}. \tag{1.17}$$

The right side of this equation will have some maximum, which will be the last point for which the equation can be solved – after that, the value of n^2 will always be greater than the right side. This is shown in figure 1.5. For a given n, this gives λ_n.

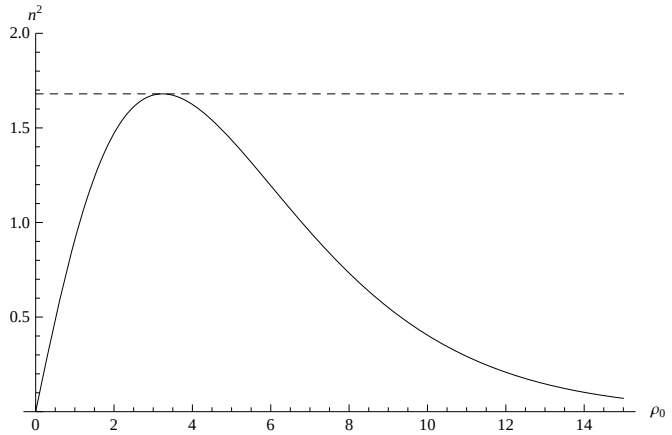

Figure 1.5: A plot of (1.17) with $\lambda = 2$, showing its maximum value. At this value of λ, the $n = 1$ bound state exists, because for $n = 1$ there is some ρ_0 that satisfies (1.17). This is not the case for the $n = 2$ bound state, so the $n = 2$ bound state does not exist. Increasing λ scales the curve, increasing the number of bound states.

To find this maximum, we differentiate with respect to ρ_0 and set the result 0, obtaining

$$0 = (1 + 2\frac{\rho_0}{\lambda_n}) - \frac{1}{\lambda_n}(\rho_0 + \frac{\rho_0^2}{\lambda_n}). \tag{1.18}$$

This is quadratic in ρ_0 and can be solved easily. As ρ_0 is a real, physical quantity that can't be negative, we can discard one solution, obtaining

$$\rho_0 = \frac{\lambda_n}{2}(1 + \sqrt{5}). \tag{1.19}$$

We can plug this in to (1.13) to find the relationship between λ and n:

$$n^2 = \lambda_n(2 + \sqrt{5})e^{-(1+\sqrt{5})/2} \Rightarrow \lambda_n = 1.19\, n^2. \tag{1.20}$$

1.5 Summary

Using the Bohr model with various assumptions to analyze the Yukawa potential yields three different expressions for the critical values λ_n: (1.11), (1.16), and (1.20). Each of these has the form

$$\lambda_n = an^2, \tag{1.21}$$

where a is some constant of order one. This suggests that when performing our numerics, we will find critical values of lambda that are proportional to the square of the number of bound states.

When applied to deuterium, we have $\lambda = 1.21245$. This suggests deuterium has exactly one bound state. However, it also implies that this bound state is unstable with $E > 0$. Given that there is a mass defect observed in deuterium, this can't quite be right. As mentioned earlier, the Bohr method does a good job of capturing qualitative behavior, but is often quantitatively inaccurate. This discrepancy between model and reality is evidently an example of the method's limitations.

Chapter 2

Numerical Methods and Results

In the previous chapter, we used semi-classical methods to analytically obtain an estimate for the number of bound states allowed by the Yukawa potential as a function of λ. We now turn our attention to the Schrödinger wave equation in order to numerically determine the critical values of λ at which new bound states appear. We will first focus on states with no angular momentum, which have spherically symmetric bound states. We will then generalize to states with non-zero angular momentum.

2.1 The Hamiltonian

Schrödinger's equation for states ψ with definite energy E can be written as

$$H\psi = E\psi, \tag{2.1}$$

where H is the Hamiltonian operator, $H = -\frac{\hbar^2}{2m}\nabla^2 + V$. We will begin by focusing on spherically symmetric bound states, so we will only be concerned with the r component of the ∇ operator. (2.1) then becomes

$$H = -\frac{\hbar^2}{2m}\left[\frac{1}{r^2}\frac{d}{dr}\left(r^2\frac{d}{dr}\right)\right] - \frac{C}{r}e^{-r/\ell}, \tag{2.2}$$

plugging in the Yukawa potential for V.

Using the same nondimensionalizations as in last chapter, we rewrite this as

$$H = \frac{C}{2\alpha}\tilde{H} = \frac{C}{2\alpha}\left[-\frac{1}{\rho^2}\frac{d}{d\rho}\left(\rho^2\frac{d}{d\rho}\right) - \frac{2}{\rho}e^{-\rho/\lambda}\right]. \tag{2.3}$$

The constant out front is the same one we used when we nondimensionalized the energy of the system, which allows us to restate (2.1) as

$$\tilde{H}\psi = \tilde{E}\psi. \tag{2.4}$$

To simplify, we can substitute

$$u(\rho) = \rho\phi(\rho) \tag{2.5}$$

into the expression in (2.3)[1]. This gives us a much neater Hamiltonian, and our differential equation is now

$$-\frac{d^2u}{d\rho^2} - \frac{2}{\rho}e^{-\rho/\lambda}u = \tilde{E}u. \tag{2.6}$$

2.2 Numerics: The Finite Difference Method

The finite difference method transforms a differential equation into a matrix problem [4]. It does this by approximating the first and second derivatives of a function on a discrete grid of points ρ_n which are a distance $\Delta\rho$ apart. The function $u(\rho)$ then becomes a function $u(\rho_n)$. The grid runs from ρ_1 to some ρ_N. Using the concept of the derivative as the slope of the tangent line at some point, we can write

$$u'(\rho_n) = \frac{u(\rho_n + \Delta\rho) - u(\rho_n - \Delta\rho)}{2\Delta\rho} - O(\Delta\rho^2), \tag{2.7}$$

$$u''(\rho_n) = \frac{u(\rho_n + \Delta\rho) - 2u(\rho_n) + u(\rho_n - \Delta\rho)}{\Delta\rho^2} - O(\Delta\rho^2). \tag{2.8}$$

Applying (2.8) to our differential equation in (2.6), we obtain

$$-u_{n-1}\frac{1}{\Delta\rho^2} - u_n\left(\frac{2}{\Delta\rho^2} - \frac{2}{\rho_n}e^{-\rho_n/\lambda}\right) - u_{n-1}\frac{1}{\Delta\rho^2} = Eu_n. \tag{2.9}$$

For the interior points there are no concerns, but at the beginning we require a u_0 and at the end we need a u_{N+1} in order to satisfy (2.9). For our problem, we set $u_0 = u(0)$ and $u_{N+1} = u(\infty)$. Our substitution $u(\rho) = \rho\psi(\rho)$ ensures that $u(0) = 0$, and our assumption that we are working with a bound state implies that $u(\infty) = 0$. Because we cannot practically calculate anything infinitely far out, we define some ρ_∞ and use $u(\rho_\infty)$ as an approximation for $u(\infty)$. We therefore require that $u_0 = u_{N+1} = 0$.

We can now construct a Hamiltonian matrix using (2.9). The matrix will have entries on the off diagonal and diagonal and nowhere else:

$$H = \begin{pmatrix} \frac{2}{\Delta\rho^2} - \frac{2}{\rho_1}e^{-\rho_1/\lambda} & -\frac{1}{\Delta\rho^2} & 0 & \dots & 0 & 0 \\ -\frac{1}{\Delta\rho^2} & \frac{2}{\Delta\rho^2} - \frac{2}{\rho_2}e^{-\rho_2/\lambda} & -\frac{1}{\Delta\rho^2} & \dots & 0 & 0 \\ 0 & -\frac{1}{\Delta\rho^2} & \frac{2}{\Delta\rho^2} - \frac{2}{\rho_3}e^{-\rho_3/\lambda} & \dots & 0 & 0 \\ \cdot & \cdot & \cdot & \dots & \cdot & \cdot \\ \cdot & \cdot & \cdot & \dots & \cdot & \cdot \\ 0 & 0 & 0 & \dots & -\frac{1}{\Delta\rho^2} & \frac{2}{\Delta\rho^2} - \frac{2}{\rho_N}e^{-\rho_N/\lambda} \end{pmatrix}.$$

The eigenvectors of this matrix will be the wave functions $u(\rho_n)$, and the eigenvalues will be the energies of the corresponding states. For the calculation of these eigenvalues and eigenvectors, we rely on Mathematica's built-in Eigenvalues[ ] command, which uses the sparsity of the matrix to optimize the calculation.

Using this, we can now see what our wave functions actually look like. For bound states where $n^2 << \lambda$, we find that the bound states look very similar to hydrogen (figure 2.1). As λ increases and more bound states are possible, the wave functions get more interesting, as in figure 2.2.

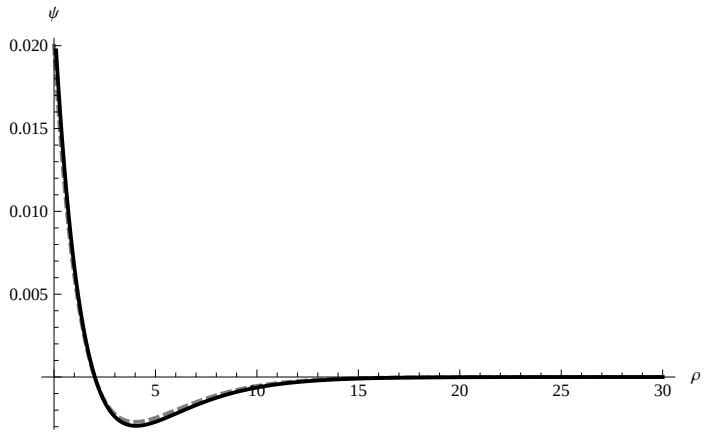

Figure 2.1: The $n = 2$ bound states for the Yukawa potential and Coulomb potential. The Yukawa potential was calculated using my finite difference Hamiltonian with $\lambda = 20$ and $\rho_\infty = 20 * 20 = 400$. The Coulomb wave function is the exact $n = 2$ wave function, scaled by a constant to match the Yukawa function. The plot only extends out to $\rho = 30$ in order to see the earlier behavior; the function remains close to 0 further out.

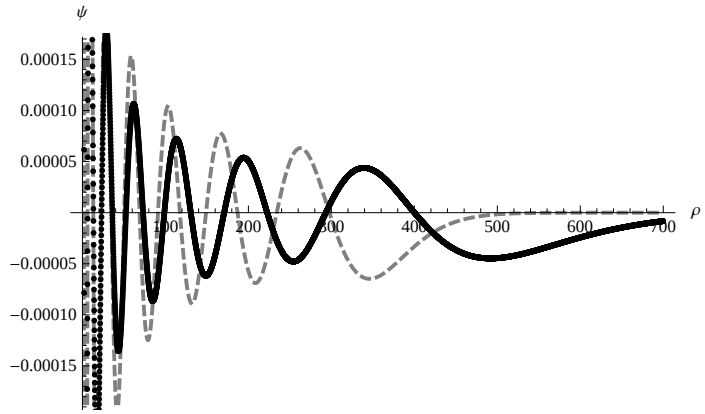

Figure 2.2: The $n = 14$ bound state at $\lambda = 200$, obtained with $\Delta\rho = 0.1$ and $\rho_\infty = 4000$. The $n = 14$ Coulomb wave function is shown as well (scaled to match). At this value of λ, the $n = 14$ state only recently became bound. This plot shows the whole range where anything interesting is going on – the function has gone to 0 and will stay there past $\rho = 700$.

2.3 Finding Critical Values of Lambda

Let us define a critical value of λ as the value of λ where the Hamiltonian matrix gains a new negative eigenvalue. λ_n will be the nth critical value, so that for $\lambda \geq \lambda_n$ we have at least n bound states with $E < 0$. This is similar to our definition in section 1.4.1, updated for the quantum mechanical case. In order to find the critical values, we calculate the number of negative eigenvalues at each value of λ and look for a place where that number increases using a variation on rootfinding. For a further discussion of the exact methods used, see Appendix A.

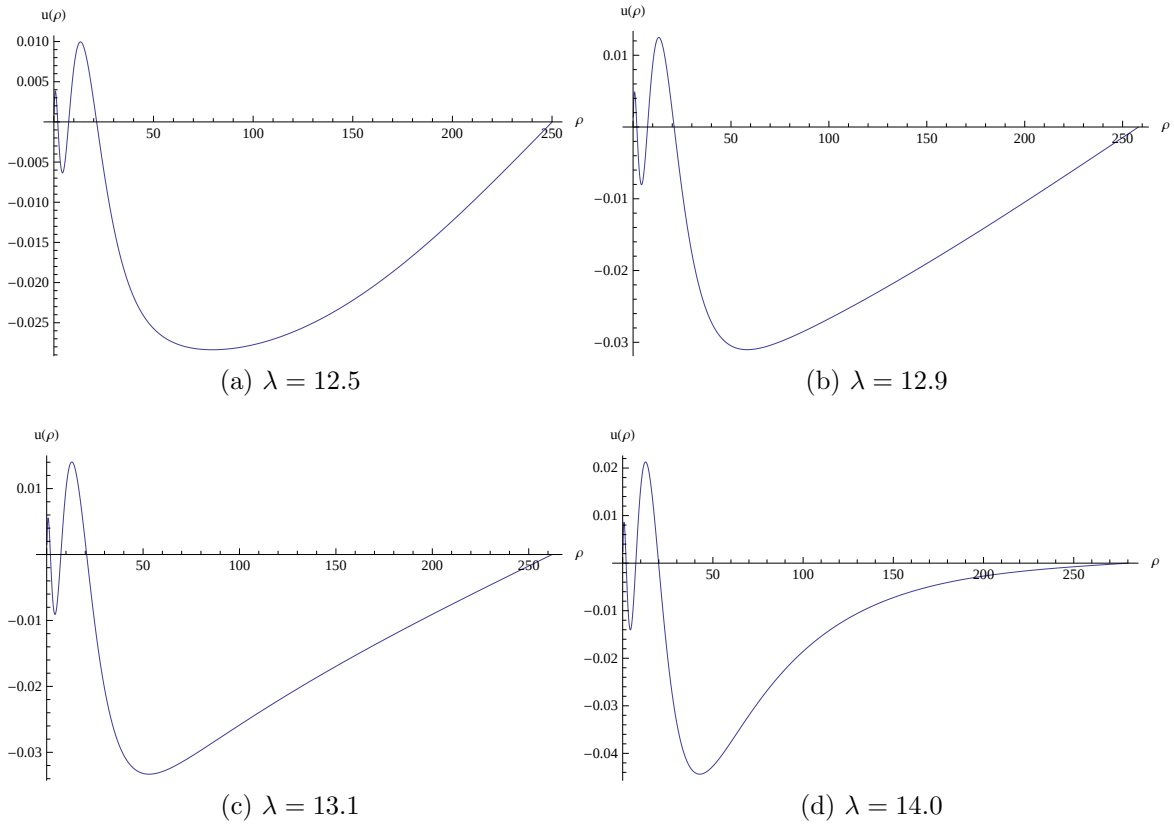

(a) $\lambda = 12.5$ (b) $\lambda = 12.9$

(c) $\lambda = 13.1$ (d) $\lambda = 14.0$

Figure 2.3: The progression of the $n = 4$ wavefunction $u(\rho)$ from scattering to bound. All wavefunctions were calculated with $\rho_\infty = 40\lambda$ and $\Delta\rho = 0.1$.

We are looking for wave functions $u(\rho)$ that behave like the ones in figure 2.3, where we plot the same state with varying λ as we pass through a critical value. In (a) the state is unambiguously scattering. While it does go to 0 at ρ_∞, this behavior is purely an artifact of the way we set up our Hamiltonian. The function primarily looks like that of a free particle in a box of size ρ_∞. In (b) it starts to level out, and in (c) the state has become bound – the function goes to zero before ρ_∞ and stays there. Finally, in (d) the state is clearly bound, going to 0 before ρ_∞.

2.4 Estimating Errors

In doing our numerical analyses, we would like to have a low $\Delta\rho$ – after all, we expect the wave function to fluctuate on length scales of order 1 with our non-dimensionalization. At the same time, we require ρ_∞ to be large, because what separates bound states from scattering states is their behavior at infinity. This puts us in the frustrating numerical position of not really having anything we can skimp on to save computation time. The values of $\Delta\rho$ and ρ_∞ are then are our two primary sources of error. To determine the errors from each, we look at how much our calculated value for some λ_n varies with changes in $\Delta\rho$ and ρ_∞.

	$\rho_\infty = 40\lambda$	$\rho_\infty = 80\lambda$	
$\Delta\rho = 0.1$	12.8255	12.7543	$\Delta\lambda_n = 0.0712$
$\Delta\rho = 0.05$	12.8233	12.7521	$\Delta\lambda_n = 0.0712$
	$\Delta\lambda_n = 0.0022$	$\Delta\lambda_n = 0.0022$	

Table 2.1: Errors in $\Delta\rho$ and ρ_∞ for λ_4.

Consider a particular critical value λ_4. We calculate the value of λ_4 at four different points: $\rho_\infty = 40\lambda$ and $\Delta\rho = 0.1$, $\rho_\infty = 40\lambda$ and $\Delta\rho = 0.05$, $\rho_\infty = 80\lambda$ and $\Delta\rho = 0.1$, and $\rho_\infty = 80\lambda$ and $\Delta\rho = 0.05$. The results of this are in table 2.1. As is seen in the table, changing $\Delta\rho$ creates the same change in λ_4 regardless of the value of ρ_∞. The reverse is also true – changes in ρ_∞ produce the same change in λ_4, regardless of the value of $\Delta\rho$. We therefore conclude that these errors are independent of each other. In addition, changes in ρ_∞ produce a much bigger change in our calculated λ_n than an equivalent change in $\Delta\rho$, at least in the ranges we are considering here. However, when sufficient errors in ρ_∞ are eliminated, errors in $\Delta\rho$ become noticeable.

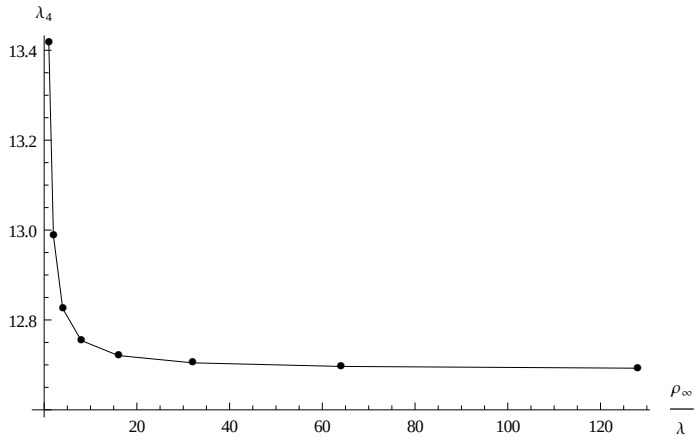

Figure 2.4: The values of λ_4 as ρ_∞ is repeatedly doubled, showing their asymptotic approach to some value. $\Delta\rho$ was held constant at 0.1. The ρ_∞ values are given in terms of ρ_∞/λ in order to make the graph more clear.

When we double ρ_∞ a few more times, we find that the calculated values of λ_n appears to asymptotically decrease, approaching some true value, as shown in figure 2.4. The size of the change in λ_4 is less than half the previous change for each doubling, indicating a rapid convergence. Because each point is closer to the true value than it is to the previous point, we can estimate the error by taking the distance between the two points. Thus, for every value of λ_n, we compute it first at some values of ρ_∞ and $\Delta\rho$, then double ρ_∞ and halve $\Delta\rho$. We use the value computed with the larger ρ_∞ and smaller $\Delta\rho$ as our data point, and the difference between the two as an estimate of our error. It is worth noting that our quoted λ_n values will all likely be too large based on this method, creating a systematic overestimate of the true value of λ_n.

2.5 Results and Fit

We ran our calculation for critical values of λ between 0.5 and 1000, using a $\Delta\rho$ of 0.1 and 0.05 and a ρ_∞ of 25000 and 50000. We found 35 critical values of λ, plotted in figures 2.5 and 2.6. The values of λ_n along with errors are given in table 2.2. At a quick glance, our data looked pretty quadratic – just what we expected. In order to explore this further, we attempted to fit the data to functions.

n	λ_n	n	λ_n	n	λ_n
1	0.843 ± 0.002	13	133.06± 0.05	25	492.0 ± 0.4
2	3.227 ± 0.002	14	154.30± 0.06	26	532.1 ± 0.5
3	7.175 ± 0.003	15	177.11± 0.08	27	573.9 ± 0.5
4	12.691± 0.003	16	201.50± 0.10	28	617.2 ± 0.6
5	19.777± 0.005	17	227.5 ± 0.1	29	662.2 ± 0.7
6	28.434± 0.007	18	255.0 ± 0.1	30	708.7 ± 0.8
7	38.663± 0.009	19	284.1 ± 0.2	31	756.8 ± 0.9
8	50.46 ± 0.01	20	314.8 ± 0.2	32	806 ± 1
9	63.84 ± 0.02	21	347.1 ± 0.2	33	858 ± 1
10	78.78 ± 0.02	22	380.9 ± 0.3	34	911 ± 1
11	95.30 ± 0.03	23	416.4 ± 0.3	35	965 ± 1
12	113.39± 0.04	24	453.4 ± 0.4		

Table 2.2: Numerically obtained critical values of λ_n for $l = 0$, with uncertanties.

Because we were looking for a relationship like $\lambda_n = an^2$, we first tried a weighted linear fit to a log-log plot (figure 2.5a). Our fit gave

$$log(\lambda_n) = -(0.2246 \pm 0.0003) + (1.9945 \pm 0.0001)\log(n). \tag{2.10}$$

The coefficient of the $\log(n)$ term isn't quite 2, and while the fit looks good, it is inaccurate, especially for low values of n. When we checked the fit against our measured error bars, the line does not pass through many of them (figure 2.5b). In addition, the residuals seemed to follow a clear pattern, suggesting something is systematically wrong with either the data or the fit. From this, we conclude that the dependence is not a pure power law.

Based on this, we decided to try a fit to the equation $\lambda_n = A + Bn + Cn^2$ (figure 2.6a). We find a general equation of

$$\lambda_n = (0.058 \pm 0.001) + (0.0518 \pm 0.0001)n + (0.785389 \pm 0.000003)n^2, \tag{2.11}$$

which matches the data much better. Residuals for this fit looked much better, with more falling inside the error bars (figure 2.6b). The residuals roughly follow the lower edges of the error bars, which is consistent with the way we asymptotically approach true values.

In comparing to published values, we are hindered by the fact that most treatments of the Yukawa potential focus on the energy spectra of states with high λ and low

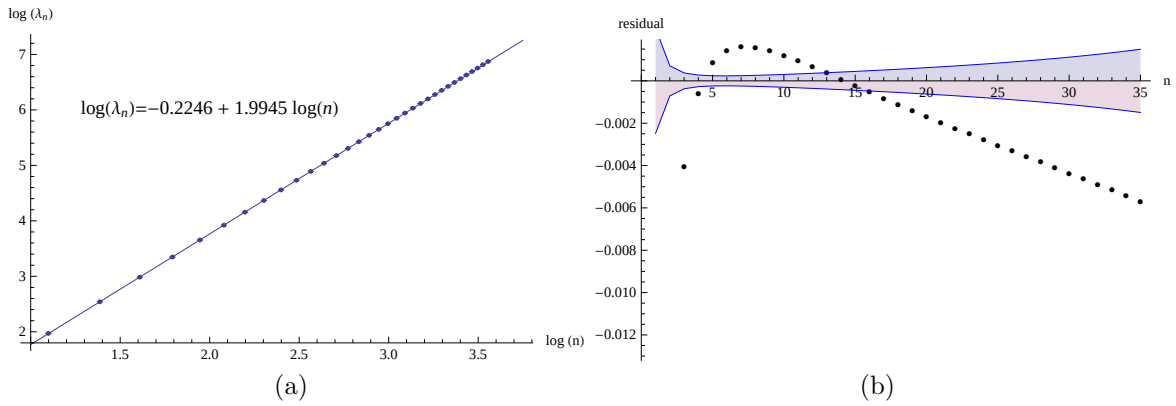

(a) (b)

Figure 2.5: Our linear fit (left) to a log-log plot of the data, with residuals (right). The residuals are the black dots, while the shaded region shows the error bars for the data points.

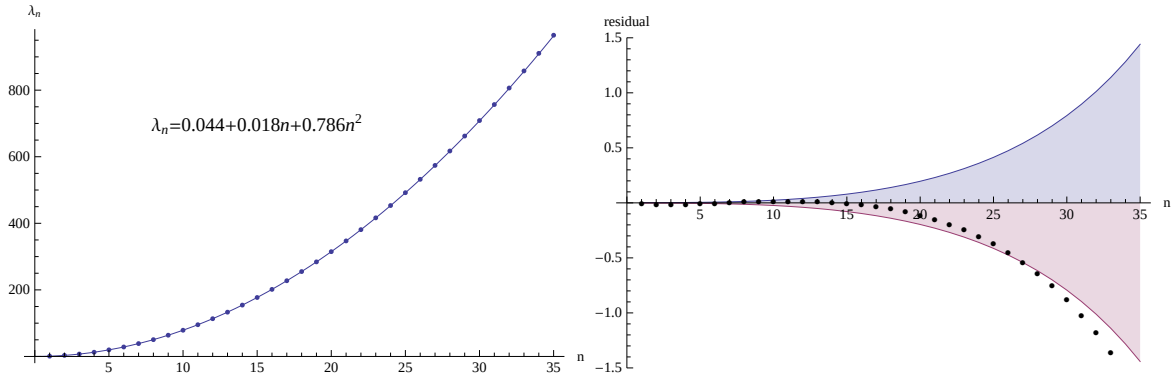

(a) (b)

Figure 2.6: Our quadratic fit (left) with residuals (right). Again, the residuals themselves are the black dots, and the shaded region shows the error bars.

n. However, there do exist published values for λ_1. Gomes, Chacham, and Mohallem find λ_1 to be $0.83990399 \pm 0.00000003$, obtained using a linear combination of atomic orbitals method [5].

This result sits just at the edge of the error bar for our results. We find λ_1 to be at least 0.841, where they find it to be at most 0.840 (rounding to the same decimal place). However, the difference is extremely small (0.01%), and our estimate is larger, which is consistent with our understanding of the systematic nature of our numerical errors.

2.6 Angular Momentum

Considering states with nonzero angular momentum is simple. Writing our wave functions as

$$\psi_{n,l,m}(\rho,\theta,\phi) = \frac{1}{\rho}u_{n,l}(\rho)Y_{l,m}(\theta,\phi), \tag{2.12}$$

the radial and angular portions separate. We update our radial equation to take into account angular momentum,

$$-u'' - \left(\frac{2}{\rho}e^{-\rho/\lambda} + \frac{l(l+1)}{\rho^2}\right)u = Eu, \tag{2.13}$$

and again discretize it using (2.8).

Following the same procedure as before, we can obtain critical values of λ for $l = 1$ to 10. These are plotted in figure 2.7 along with the $l = 0$ data from the previous section.

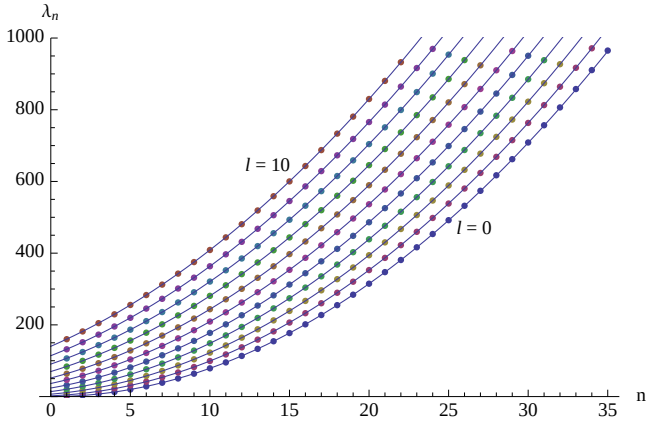

Figure 2.7: The relationship between λ_n and n for $l = 0$ to 10. In this plot, n is the radial quantum number. The principal quantum number is now $l + n$. To obtain these curves, we chose to fix $\Delta\rho$ at 0.1, and set ρ_∞ to 80λ.

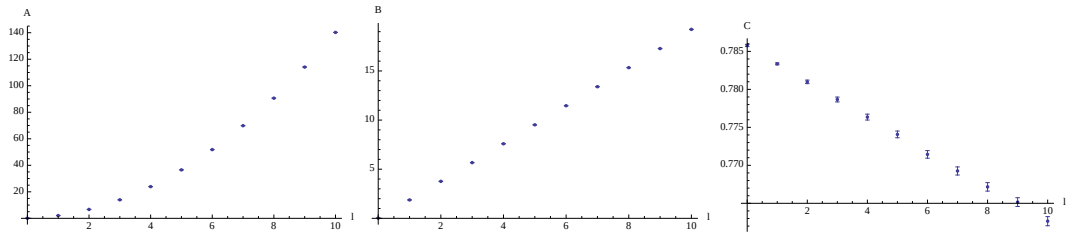

(A) (B) (C)

Figure 2.8: Three graphs showing the changes in fit parameters A, B, and C as a function of l.

Again, all the curves neatly fit a quadratic, giving fit functions in the form $\lambda_n = A + Bn + Cn^2$. The constants of the quadratic are dependent on l and listed in

table 2.3. B and C appear to vary linearly with l, while A seems to vary quadratically. This is shown in figure 2.8.

Table 2.3: The fit parameters A, B, and C (with uncertainties) for $l = 0$ to 10.

l	A	B	C
0	0.058 ± 0.001	0.0518 ± 0.0001	0.785389 ± 0.000003
1	2.08 ± 0.03	1.872 ± 0.004	0.7834 ± 0.0001
2	6.70 ± 0.06	3.762 ± 0.008	0.7810 ± 0.0002
3	13.97 ± 0.07	5.67 ± 0.01	0.7787 ± 0.0003
4	23.92 ± 0.08	7.59 ± 0.01	0.7763 ± 0.0004
5	36.55 ± 0.09	9.52 ± 0.01	0.7741 ± 0.0004
6	51.84 ± 0.09	11.46 ± 0.01	0.7714 ± 0.0005
7	69.88 ± 0.09	13.40 ± 0.01	0.7693 ± 0.0005
8	90.62 ± 0.08	15.34 ± 0.01	0.7672 ± 0.0006
9	114.08 ± 0.08	17.28 ± 0.01	0.7652 ± 0.0006
10	140.22 ± 0.07	19.23 ± 0.01	0.7626 ± 0.0006

We note that when l is non-zero, the quantum number n is actually the *radial* quantum number. Our numerical procedure finds the lowest energy state for a given value of l, and labels that state with $n = 1$. The next is then $n = 2$, and so on. The principal quantum number then becomes $n_p = n + l$. Thus, at principal quantum number $n_p = 1$, we require that $l = 0$. At $n_p = 2$, we can have $l = 0$ or $l = 1$.

Accordingly, the bound states at higher l start further away from the origin at a higher value of λ. This explains some of the dependence of A, B, and C on l, if we assume that λ should actually be quadratic in n_p. In this case we can write

$$\lambda_{n_p} = \tilde{A} + \tilde{B}n_p + \tilde{C}n_p^2 = \tilde{A} + \tilde{B}(n + l) + \tilde{C}(n + l)^2. \tag{2.14}$$

When we do this, we obtain the plot of λ_{n_p}s shown in figure 2.9. These parameters are closer to constant, but we can see that they still have some remaining dependence on l.

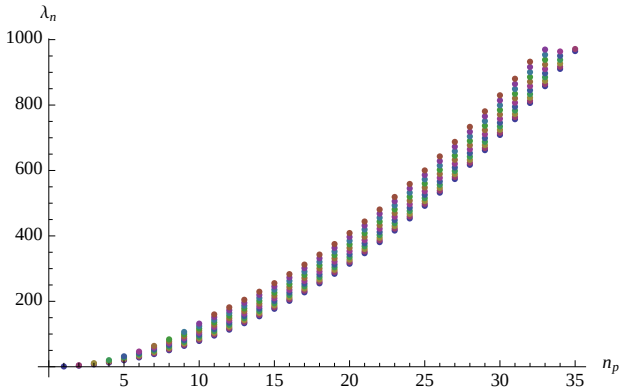

Figure 2.9: These curves show the relationship between λ_n and $n_p = n + l$ for $n_p = 0$ to 35.

Conclusions

The Yukawa potential has only a finite number of bound states. The potential decreases to zero quickly outside of a region described by λ, the ratio between the exponential cutoff length scale ℓ and the "Bohr radius" α. Any state sitting too far from the origin compared to this length scale cannot be bound, because there is not enough force to bind it. This implies that the number of bound states increases with increasing λ, and we can define a critical value λ_n as the value of λ at which the nth bound state appears. We first used the Bohr model to get an approximate relationship between the number of bound states of the Yukawa potential and the value of the length scale. We then obtained the same relationship directly from the potential using the finite difference method. As with other central force potentials, the Bohr method gave a reasonable approximation, but the numerical picture was more subtle. We found that the relationship between the number of bound states n and the non-dimensionalized length scale λ was of the form $\lambda_n = A(l) + B(l)n + C(l)n^2$, where A, B, and C are constants dependent on the quantum number l.

While this method was intended to look at the number of bound states, not the energies, a possible extension of this work would be to obtain an energy spectrum at some value of λ. However, in order to do this, one would need a different routine for finding the eigenvalues of the Hamiltonian matrix, as the continuous eigenvalues above zero create computational challenges. We could also extend this work to investigate the unstable bound states – those states with $E > 0$ that are still partially bound. These states should primarily occur at higher values of λ, and should be distinguishable from pure scattering states.

Appendix A

Numerical Methods

A.1 Rootfinder

To actually locate the critical values of λ, we need to find the place where a new bound state appears. Numerically, this looks like a new negative eigenvalue in our list of eigenvalues, which suggests we approach the problem with rootfinding. Our function has a "zero" whenever the number of negative eigenvalues increases.

Here it is in *Mathematica* code:

```
Critical[λ_, consts_] :=  Module[{H, res, dρ, ρinf, nn},
    dρ = consts[[1]];
    ρinf = Round[consts[[2]]];
    nn = Round[ρinf/dρ];
    H = SparseArray[{{n_, n_} ->
        2./dρ^2 - 2./(n*dρ) e^(-n*dρ/λ) + (
        l (l + 1))/(n*dρ)^2, {n_, m_} /; Abs[n - m] == 1 -> -1./
        dρ^2}, {nn, nn}, 0.];
    res = Sort[Eigenvalues[H, -25]];
    Return[res]
  ]
```

This function takes a value of lambda and returns some number of eigenvalues (here, 25) of the Hamiltonian which have the lowest absolute value. nn is the matrix size, dρ is the step size, and ρinf is numerical infinity for the problem.

The results of this calculation are extremely sensitive to ρinf, and a larger ρinf makes for less error. However, for larger values of ρinf, more positive eigenvalues are found near 0, because the positive eigenvalues are in a continuous spectrum. As the grid becomes a better approximation of reality, more of these are picked up. This squeezes the negative eigenvalues (whose spectrum starts near -1) out, especially at higher values of λ. In order to ensure that there are *some* negative eigenvalues, we therefore pin ρinf to some constant factor times λ.

Increasing the number of negative eigenvalues found will also ensure we don't miss negative eigenvalues, but is very expensive. When searching for initial eigenvalues,

we chose to get the 100 with the lowest absolute value in order to increase accuracy, but for the main calculation, 25 was fine.

The rootfinder actually used was a recursive bisection routine. In this rootfinder, we stopped recursing when the difference between the two endpoints was less than some δ, instead of when the values of the function at the endpoints were within ϵ. Because our function just looks at the number of negative eigenvalues, $f(\lambda_f) - f(\lambda_0)$ should always be equal to 1 in a range with a zero and ϵ is meaningless.

In *Mathematica* code:

```
Bisect[F_, consts_, x0_, xf_, ϵ_] := Module[{mid, val, lnegs, vam, mnegs, vah},
    mid = x0 + Abs[x0 - xf]/2;
    Print["Bisecting. Midpoint is " <> ToString[mid]]; (*progress indicator*)
    val = F[x0, consts];
    lnegs = CountNegs[val];
    vam = F[mid, consts];
    mnegs = CountNegs[vam];
    If[xf - x0 > ϵ,
        If[lnegs < mnegs || (lnegs == mnegs && val[[1]] < vam[[1]]),
            Return[Bisect[F, consts, x0, mid, ϵ]];,
            Return[Bisect[F, consts, mid, xf, ϵ]];
     ];,
   vah = F[xf, consts];
   Return[mid, lnegs, CountNegs[vah]];
   ]
]
```

Again, when we bisect, we are looking at the number of negative eigenvalues as a function of lambda. In this routine, we assume multiple zeroes and keep bisecting any range with a zero in it.

The complicated conditional for bisection is meant to deal with the problem of negative eigenvalues getting squeezed out by positive ones. Given half of the input range, it bisects that half if either the number of negative eigenvalues increases (a regular zero), or the number of negative eigenvalues stays constant but the value of the first negative eigenvalue jumps. This indicates that one negative eigenvalue was squeezed out, but another was added. In general, as λ increases, the negative eigenvalues should decrease in value (coming closer and closer to the Coulomb energies).

To find the ranges to bisect, we modify the rootfinder so it keeps bisecting as long as there is a zero in one of the ranges, and returns a list of points instead of just one. For efficiency's sake, this calculation is run at a low ρ_∞, and a range is returned instead of a single point. That range can then be bisected more thoroughly in order to identify the most likely point.

As is clear from the code, the function doing the actual work is just Mathematica's Eigenvalues[ ]. Because our Hamiltonian matrix only has entries on the diagonal and off-diagonals, we can define it as a SparseArray to speed up calculation.

Finding a single λ_n takes quite a bit of time – it's expensive to find the eigenvalues of a large matrix, even such a sparse one as ours. We would like to study a wide

range of λs, and the computation begins to look prohibitively expensive. However, the problem is embarrassingly parallel. Each bisection to find a value of λ_n is independent of all the others, allowing us to easily split this problem into chunks. We used Mathematica's Lightweight Grid to run the computation on a cluster of machines. Distributing these calculations among multiple cores speeds the process up by about 50% per core added.

A.2 Fits

A.2.1 Linear

Our weighted linear least-squares fit was computed following the methods outlined in Taylor [6]. We first compute weights for each point, based on its error, then use that to weight the least-squares calculation.

Here it is in Mathematica code:

```
weights = Table[1/(logerrs[[i]]^2), {i, 1, Length[logerrs]}];

x[i_] := loglog[[i, 1]];
y[i_] := loglog[[i, 2]];
w[i_] := weights[[i]];
len = Length[loglog]

Delta = Sum[w[[i]], {i, len}]*Sum[w[[i]]*x[i]^2, {i, len}] -
        (Sum[w[[i]]*x[i], {i, len}])^2;

A = 1/Delta*(
        Sum[w[i]*x[i]^2, {i, len}] *Sum[w[i]*y[i], {i, len}] -
        Sum[w[i]*x[i], {i, len}]*Sum[w[i]*x[i]*y[i], {i, len}])

B = 1/Delta*(
        Sum[w[i], {i, len}]*Sum[w[i]*x[i]*y[i], {i, len}] -
        Sum[w[i]*x[i], {i, len}]*Sum[w[i]*y[i], {i, len}])
```

A.2.2 Quadratic

For our quadratic fit, we first decided to ignore data weights as the errors were largely on similar orders of magnitude. Instead of calculating the coefficients of the fit independently, we did it with a matrix inversion, because the expressions for each component are complicated. More precisely, we solved the equation

$$\begin{pmatrix} N & \sum n_i & \sum n_i^2 \\ \sum n_i & \sum n_i^2 & \sum n_i^3 \\ \sum n_i^2 & \sum n_i^3 & \sum n_i^4 \end{pmatrix} \begin{pmatrix} A \\ B \\ C \end{pmatrix} = \begin{pmatrix} \sum \lambda_i \\ \sum n_i \lambda_i \\ \sum n_i^2 \lambda_i \end{pmatrix}. \tag{A.1}$$

for A, B, and C. For the matrix inversion, we just used the one built into Mathematica.

When we turned this into a weighted fit, we picked up some extra $\Delta\lambda_i$ terms:

$$\begin{pmatrix} \sum \frac{1}{\Delta\lambda_i^2} & \sum \frac{n_i}{\Delta\lambda_i^2} & \sum \frac{n_i^2}{\Delta\lambda_i^2} \\ \sum \frac{n_i}{\Delta\lambda_i^2} & \sum \frac{n_i^2}{\Delta\lambda_i^2} & \sum \frac{n_i^3}{\Delta\lambda_i^2} \\ \sum \frac{n_i^2}{\Delta\lambda_i^2} & \sum \frac{n_i^3}{\Delta\lambda_i^2} & \sum \frac{n_i^4}{\Delta\lambda_i^2} \end{pmatrix} \begin{pmatrix} A \\ B \\ C \end{pmatrix} = \begin{pmatrix} \sum \frac{\lambda_i}{\Delta\lambda_i^2} \\ \sum \frac{n_i\lambda_i}{\Delta\lambda_i^2} \\ \sum \frac{n_i^2\lambda_i}{\Delta\lambda_i^2} \end{pmatrix}. \tag{A.2}$$

Appendix B

Data

Table B.1: All the critical values λ_n for non-zero l.

n	$l=1$	$l=2$	$l=3$	$l=4$	$l=5$	$l=6$	$l=7$	$l=8$	$l=9$	$l=10$
1	4.541	10.947	20.068	31.904	46.459	63.730	83.720	106.428	131.854	159.999
2	8.872	17.210	28.257	42.018	58.496	77.691	99.604	124.235	151.583	181.650
3	14.730	24.984	37.949	53.630	72.028	93.143	116.977	143.528	172.798	204.786
4	22.130	34.285	49.159	66.752	87.064	110.096	135.847	164.318	195.507	229.414
5	31.080	45.121	61.894	81.392	103.614	128.558	156.224	186.609	219.715	255.540
6	41.585	57.501	76.163	97.559	121.684	148.536	178.112	210.410	245.430	283.170
7	53.647	71.427	91.970	115.257	141.281	170.035	201.517	235.725	272.655	312.308
8	67.270	86.905	109.321	134.493	162.409	193.061	226.445	262.558	301.396	342.959
9	82.455	103.937	128.219	155.268	185.071	217.617	252.899	290.913	331.657	375.127
10	99.204	122.525	148.666	177.588	209.272	243.706	280.883	320.795	363.440	408.814
11	117.516	142.670	170.664	201.453	235.014	271.333	310.399	352.206	396.750	444.025
12	137.394	164.375	194.217	226.867	262.300	300.499	341.451	385.150	431.588	480.762
13	158.838	187.641	219.325	253.832	291.132	331.207	374.042	419.628	467.959	519.028
14	181.848	212.468	245.990	282.349	321.512	363.459	408.172	455.643	505.863	558.826
15	206.425	238.857	274.212	312.419	353.442	397.256	443.846	493.198	545.303	600.156
16	232.569	266.809	303.994	344.045	386.923	432.602	481.063	532.293	586.282	643.022
17	260.281	296.325	335.336	377.226	421.956	469.496	519.826	572.931	628.800	687.425
18	289.560	327.406	368.238	411.965	458.543	507.941	560.136	615.113	672.860	733.367
19	320.407	360.051	402.701	448.262	496.685	547.937	601.995	658.841	718.462	780.849
20	352.823	394.261	438.727	486.118	536.382	589.486	645.403	704.116	765.609	829.873
21	386.807	430.037	476.315	525.533	577.636	632.588	690.363	750.939	814.302	880.440
22	422.359	467.379	515.467	566.508	620.447	677.245	736.874	799.311	864.541	932.551
23	459.480	506.287	556.182	609.045	664.817	723.458	784.938	849.233	916.328	-
24	498.170	546.761	598.461	653.142	710.745	771.227	834.555	900.707	969.664	-
25	538.429	588.802	642.304	698.802	758.233	820.552	885.727	953.733	-	-
26	580.257	632.410	687.712	746.023	807.280	871.435	938.455	-	-	-
27	623.654	677.585	734.684	794.808	857.888	923.877	-	-	-	-
28	668.620	724.328	783.223	845.156	910.057	-	-	-	-	-
29	715.156	772.637	833.326	897.067	963.787	-	-	-	-	-
30	763.261	822.515	884.995	950.542	-	-	-	-	-	-
31	812.935	873.960	938.231	-	-	-	-	-	-	-
32	864.179	926.973	-	-	-	-	-	-	-	-
33	916.992	-	-	-	-	-	-	-	-	-
34	971.375	-	-	-	-	-	-	-	-	-
35	-	-	-	-	-	-	-	-	-	-

References

[1] D. J. Griffiths, *Introduction to quantum mechanics* (Pearson Prentice Hall, Upper Saddle River, NJ, 2005).

[2] S. L. Garavelli and F. A. Oliveira, Phys. Rev. Lett. **66**, 1310 (Mar 1991), `http://link.aps.org/doi/10.1103/PhysRevLett.66.1310`.

[3] T. Garon, *The Two-Dimensional Hydrogen Atom*, Reed thesis, Reed College (2011).

[4] W. H. Press, S. A. Teukolsky, W. T. Vetterling, and B. P. Flannery, *Numerical Recipes 3rd Edition: The Art of Scientific Computing* (Cambridge University Press, 2007).

[5] O. A. Gomes, H. Chacham, and J. R. Mohallem, Phys. Rev. A **50**, 228 (Jul 1994), `http://link.aps.org/doi/10.1103/PhysRevA.50.228`.

[6] J. R. Taylor, *An introduction to error analysis : the study of uncertainties in physical measurements* (University Science Books, Sausalito, Calif., 1997).

[7] R. Eisberg and R. Resnick, *Quantum Physics of Atoms, Molecules, Solids, Nuclei, and Particles* (Wiley, 1985).